Comparison of Small-Angle Scattering Methods for the Structural Analysis of Octyl-β-maltopyranoside Micelles

Lizhong He,[†] Vasil M. Garamus,[†] Sérgio S. Funari,[‡,§] Marc Malfois,[∥,⊥] Regine Willumeit,[†] and Bernd Niemeyer*[,†,▽]

Institute for Coastal Research/Physical and Chemical Analysis, GKSS National Research Center, D-21502 Geesthacht, Germany, Universität Rostock, Physics Department, c/o HASYLAB, D-22603 Hamburg, Germany, European Molecular Biology Laboratory, Hamburg Outstation, D-22603 Hamburg, Germany, and Universität der Bundeswehr Hamburg, D-22043 Hamburg, Germany

Received: January 9, 2002; In Final Form: April 23, 2002

Small-angle neutron scattering (SANS) and small-angle X-ray scattering (SAXS) experiments were performed to investigate the micelle structure of *n*-octyl-β-maltopyranoside (OM). Density measurements were carried out to obtain the volumetric characteristics of OM for micelle structure analysis. Both temperature and concentration were varied in scattering experiments to study their effects on micelle size. The scattering data were analyzed by the indirect Fourier transformation method (IFT) and model fitting. The IFT method gave the radius of gyration of the micelles and their pair distance distribution function. It was found that the radii of gyration from SANS data were much smaller than those from SAXS data at similar solution conditions. Moreover, pair distance distribution functions from SANS and SAXS data were also different. Model fitting indicated that a spherical shell model can be used to describe both SANS and SAXS data using similar structure parameters. Comparison of SAXS data in D_2O and H_2O shows that the OM micelle has a similar structure in both solvents. The size of the micelle does not increase with increasing concentration up to 188 mM. From 10 to 50 °C, the structure of the micelle is not sensitive to temperature changes. Comparison of the micelle structures of OM with those of its two closely related glycolipids, *n*-octyl-β-glucopyranoside (OG) and *n*-dodecyl-β-maltopyranoside (DM), suggests that the hydrophilic force plays an important role in the micelle structure of glycolipids.

Introduction

Glycolipids are amphiphilic molecules containing saccharide residues linked to a hydrophobic moiety. They are of great interest not only because of their important physiological function (cell recognition) but also because of their extensive application.[1,2] Glycolipids such as *n*-octyl-glucopyranoside (OG), *n*-octyl-maltopyranoside (OM), and *n*-dodecyl-maltopyranoside (DM) have been used as biosurfactants in biology and biotechnology.[3−5] For example, they have been utilized extensively in biochemical membrane research to solubilize and isolate membrane proteins.[6−9] In environmental technology, glycolipids are employed in the treatment of pollutants and are less environmentally damaging than many other synthetic surfactants.[10,11] Because these glycolipids can be produced from renewable sources, they are usually referred to as natural surfactants.[12]

Knowledge of the physicochemical properties of natural surfactants enables a better understanding of their applications in biological and environmental processes.[12] Therefore, the phase and aggregation behavior of glycolipids (e.g., alkyl glucopyranosides and alkyl maltopyranosides) have attracted the interest of many researchers.[13−22] Recently, decyl- and dodecyl-maltopyranosides have been studied by different authors.[16,19−22] The properties of OM, however, have not been thoroughly investigated despite its wide utilization. Until now, reports can be found in the literature only on a few of its properties, such as thermotropic phase behavior and CMC (critical micelle concentration).[23−26] It has been found that up to a concentration of 60% and over a temperature range from 0 to 100 °C only an L_1 phase exists in the OM−water system.[23]

The present work was done to study the micelle structure of OM. To this end, SANS, SAXS, and volumetric methods were combined to obtain detailed insight into micelle formation. The combination of SANS and SAXS can provide excellent elucidation of the micelle structure because of complementary information that can be obtained from these techniques.[13−15,27] Here, the results of these two experimental methods were compared in the structure investigation of OM micelles. For the analysis of scattering data, a free-form method and model fitting methods were used with SANS and SAXS data to obtain different information about the micelle structure.

It is known that chain lengths and the degree of glucosidation are essential parameters that dominate the phase and aggregation behavior of glycolipids.[13−15,21−24] Hence, it is interesting to compare the micelle structures of OM with those of its two closely related glycolipids, OG (1 sugar in the head and 8 carbons in the tail) and DM (2 sugars in the head and 12 carbons in the tail). Molecular structures of these three glycolipids are

* Corresponding author. E-mail: bernd.niemeyer@gkss.de. Fax: (0049)-4152-871909.
[†] GKSS National Research Center.
[‡] Univesität Rostock.
[§] Present address: Max-Planck Institute for Colloids and Interfaces, c/o HASYLAB, D-22603 Hamburg, Germany.
[∥] European Molecular Biology Laboratory.
[⊥] Present address: DUBBLE CRg-ESRF, BP 220, F-38043, Grenoble, France.
[▽] Universität der Bundeswehr Hamburg.

10.1021/jp020034o CCC: $22.00
Published on Web 07/10/2002

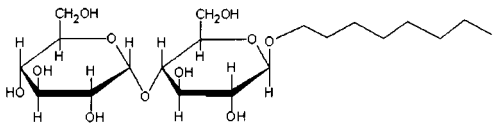

OM

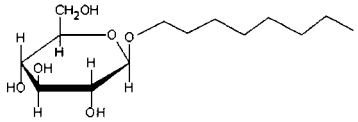

OG

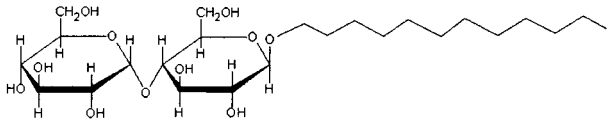

DM

Figure 1. Chemical structures of *n*-octyl-β-maltoyranoside (OM), *n*-octyl-β-glucopyranoside (OG), and *n*-dodecyl-β-maltopyranoside (DM).

shown in Figure 1. The micelle structures of OG and DM have been reported in refs 17 and 19.

Materials and Methods

Materials. OM (purity >98%) was purchased from Sigma Chemical Co. (St. Louis, MO). It was dried by lyophilizing overnight before preparing the working solutions. D_2O (deuteration grade >99.8%) was obtained from Merck Co. (Merck, Germany). A high-purity water system was used to produce H_2O with a conductivity lower than 0.05 μS.

Density and Volumetric Properties. Densities, ρ, were measured using a vibrating method with a DMA 4500 density meter (Anton Paar, Graz, Austria). From the measured density, the apparent molar volume of OM, V_ϕ, was calculated from

$$V_\Phi = \frac{\mathrm{MW}}{\rho'} - \frac{1000(\rho' - \rho_0')}{m\,\rho_0'\rho'} \tag{1}$$

where MW is the molar mass of the solute, *m* is the molality of the solution, ρ' is the mass density of the solution, and ρ_0' is the mass density of the solvent. Partial molar volumes of the solutes, $\bar{V}$, can be calculated with the relation

$$\bar{V} = \left(\frac{\partial(V_\Phi m)}{\partial m}\right)_{T,P} \tag{2}$$

The following equation was employed to describe the change of the apparent molar volume with concentration:[28]

$$V_\Phi = V_\Phi^0 + am^{1/2} + bm \tag{3}$$

The values of the parameters *a* and *b* were obtained by fitting the experimental apparent molar volume data. By combining eqs 2 and 3, one can obtain

$$\bar{V} = V_\Phi^0 + \frac{3}{2}am^{1/2} + 2bm \tag{4}$$

Thus, the partial molar volumes of OM at different concentrations can be obtained using the known parameters *a* and *b*. Note that the value of the parameters *a* and *b* were applied only in the measured concentration region. Outside this region, they may be invalid.

The volume of the hydrocarbon chains at 25 °C was calculated using the Tanford method:[29]

$$v_c = 27.4 + 26.9n_c \tag{5}$$

n_c is the number of carbon atoms in the hydrocarbon chains. Using the value calculated by eq 5 as a reference, the volume of the hydrocarbon chains at other temperatures was obtained by correlation methods (see Supporting Information).

SANS Experiments. The SANS experiments were performed on the instrument SANS-1 at the Geesthacht Neutron Facility GeNF, Geesthacht, Germany. Four sample-to-detector distances (from 0.7 to 7 m) were employed to cover the range of scattering vectors *q* ($q = 4\pi \sin\theta/\lambda$, where 2θ is the scattering angle and λ is the wavelength) from 0.007 to 0.25 $Å^{-1}$. In all experiments, the neutron wavelength λ was 8.5 Å with a wavelength resolution, $\Delta\lambda/\lambda$, of 10% (full width at half-maximum value). To ensure that the experiments were performed under isothermal conditions, the quartz cuvettes (1-mm path length) containing the sample solutions were placed in a thermostated sample holder.

The raw data was corrected for background contributions from the solvent and sample cell by conventional procedures.[30] The 2D isotropic scattering patterns were azimuthally averaged, converted to an absolute scale, and corrected for detector efficiency by using the incoherent scattering pattern of pure water,[31] which was measured with a 1-mm path length quartz cell. The smearing induced by the instrumental setup was considered in the later data analysis.[32]

SAXS Experiments. The SAXS experiments were performed on the instrument X33 NCS at the European Molecular Biology Laboratory (EMBL) outstation in Hamburg, Germany.[33,34] The experiments were performed using an X-ray wavelength of 1.5 Å. The scattering intensities were collected with a position-sensitive gas detector. The data were normalized with respect to the incident beam and were corrected for positional detector sensitivity variations. Scattering due to the buffer, which was measured before and after every sample measurement, was subtracted. The statistical error propagation was determined using SAPOKO (Svergun, D. I. and Koch, M. H. J., unpublished work) and OTOKO programs, which can be obtained from the EMBL web site.[35]

Analyses of SANS and SAXS Data

Free-Form Method. Free-form methods are model-independent approaches, which are well suited to the qualitative analysis of scattering data.[36,37] In this work, we show results obtained by the IFT method, introduced by Glatter, which is such a free-form method.[38] In the IFT method, the radius of gyration of the particles is given by[38,39]

$$R_g^2 = \frac{\int_0^{D_{\max}} p(r)\, r^2\, \mathrm{d}r}{2\int_0^{D_{\max}} p(r)\, \mathrm{d}r} \tag{6}$$

where $D_{\max}$ is the upper limit for the maximum particle dimension and $p(r)$ is the pair distance distribution function of a particle. R_g as defined by eq 6 differs from the usual definition, $\ln(I) \sim q^2R_g^2/3$, because $p(r)$ depends on the scattering-length

density profile. Note that the definition given in eq 6 is extensively used in numerical calculations by IFT.[38,39] The $p(r)$ function is approximated by a linear combination of a finite number of cubic B-spline functions $\varphi_i(r)$

$$p(r) = \sum_{i=1}^{N} c_i \varphi_i(r) \tag{6a}$$

where the expansion coefficients c_i are fitting parameters determined from the scattering data. A large number ($N = 20-30$) of functions $\varphi_i(r)$ are used to describe the $p(r)$ function. The IFT method requires no presumption of the shape of the particle. In the present study, the values of D_{max} were carefully chosen to ensure accurate fits of the experimental data and to obtain smooth $p(r)$ functions. For each set of experimental data, the calculation results using different D_{max} values at intervals of 2 Å were compared, and the value corresponding to the best fit and a smooth $p(r)$ function was chosen.

Model Fitting. The IFT method provides useful information such as the radius of gyration and the $p(r)$ function, but the obvious goal is to obtain specific structural parameters by fitting the model to the data. Micelles are composed of a hydrophobic core and a hydrophilic shell, and because these two parts normally have different scattering length densities, it is appropriate to use shell models to describe their shapes.[36] In the present work, a spherical, an ellipsoidal, and a cylindrical shell model have been used to fit the data. For slightly anisotropic or polydisperse particles, the scattering cross section, $\frac{d\Sigma(q)}{d\Omega}$, can be described in a decoupling approximation by[40]

$$\frac{d\Sigma(q)}{d\Omega} = nP(q)S'(q) \tag{7}$$

where

$$P(q) = \langle |F(q)|^2 \rangle \tag{8}$$

$$S'(q) = 1 + \beta(q)[S(q) - 1] \tag{9}$$

$$\beta(q) = |\langle F(q) \rangle|^2 / \langle |F(q)|^2 \rangle \tag{10}$$

The inner brackets $\langle\ \rangle$ in eqs 8 and 10 respectively represent an average weighted by the distribution of particle sizes or orientation, n is the number density (corresponding to the concentration) of the particles in the solution, $P(q)$ is the form factor, $F(q)$ is the amplitude of the form factor, $S(q)$ is the structure factor, and $S'(q)$ is the effective structure factor modified by the anisotropy and polydispersity of the particles. For a two-shell particle, $F(q)$ is written as[36,41]

$$F(q) = V_c(\rho_c - \rho_s)\, f(q, V_c, \text{sh}) + (V_s + V_c)(\rho_s - \rho_0)\, f(q, V_c + V_s, \text{sh}) \tag{11}$$

where V_c is the volume of the micelle core, V_s is the volume of the hydrophilic shell, ρ_c is the scattering density of the micelle core, ρ_s is the scattering density of the hydrophilic shell, ρ_0 is the scattering density of the solvent, and the function $f(q, V, \text{sh})$ depends on the volume (size) and the shapes (sh) of the micelle core and the total micelle.

For an ellipsoid of revolution with three semiaxes b, b, and a ($a = \epsilon \cdot b$), function $f(q, V, \text{sh})$ is expressed by

$$f(q, V, \text{sh}) = f(x) = 3[\sin(x) - x\cos(x)]/(x)^3 \tag{12}$$

where $x = qb[\sin^2\beta + \epsilon^2 \cos^2\beta]^{1/2}$ and β is the angle between the vector q and the axis of the particle. For $\epsilon = 1$, eq 12 describes the scattering of the sphere of radius b.

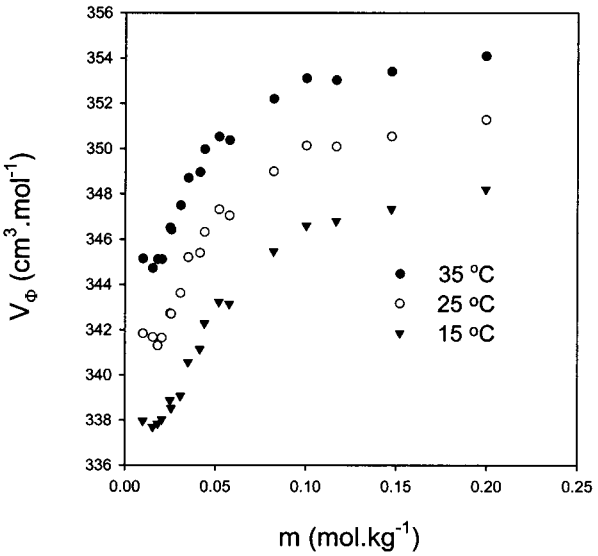

Figure 2. Dependence of the apparent molar volume of OM, V_ϕ, on concentration (m) at different temperatures.

For a cylinder, $f(q, V, \text{sh})$ is written as

$$f(q, V, \text{sh}) = \frac{\sin(qL/2\cos\beta)\, 2J_1(qR\sin\beta)}{(qL/2\cos\beta)(qR\sin\beta)} \tag{13}$$

where L is the length of the cylinder, R is the radius of the cylinder, and J_1 is the first-order Bessel function.[36] The structure factor $S(q)$ can been calculated with the Percus−Yevick approximation for the closure relation:[42]

$$S(q) = \frac{1}{1 + 24\eta_{HS}\, G(qR_{HS})/qR_{HS}} \tag{14}$$

η_{HS} is the hard sphere volume fraction, and R_{HS} is the hard-sphere radius. The detailed expression of the function $G(qR_{HS})$ in eq 14 can be found in the literature.[42,43] The value of the hard sphere radius R_{HS} was set to be the radius of a corresponding spherical particle, which volume is identical to that of the particle studied. The calculated and experimental intensities were compared by the least-squares method.[32] The parameters in the models were optimized and the statistical errors were calculated by conventional methods.[44]

Results

Volumetric Properties. Volumetric properties are useful in analyzing micelle structure. Figure 2 shows the measured apparent molar volume of OM at 15, 25, and 35 °C. From these data, the partial molar volume of the solute was calculated with eq 4. With the volume of the hydrocarbon chains calculated by the Tanford method,[29] the head group volume was obtained. Table 1 summarizes the volumetric characteristics of the OM molecule at different temperatures. These volumes are used to calculate the scattering-length density, aggregation number, and hydration number. The reader is referred to section 1s of the Supporting Information for more volumetric data at other temperatures.

Comparison of SANS and SAXS Data. Typical SAXS and SANS patterns are shown in Figure 3a. The $p(r)$ functions obtained by the IFT method are shown in Figure 3b. In Figure 3a, there is a peak around $q = 0.37$ Å^{-1} in the SAXS pattern

TABLE 1: Molecular Volume Properties of OM

temperature (°C)	molecular volume[a] v_{mol} (Å^3)	carbon chain volume[b] v_c (Å^3)	head group volume[c] v_h (Å^3)
15	582.4	239.8	342.6
25	587.3	242.6	344.7
35	591.7	245.5	346.2

[a] The partial molar volume at 100 mM was used to calculate the molecular volume. [b] The value at 25 °C was calculated using $v_c = 27.4 + 26.9n_c$, and temperature correlation was carried out to obtain the value at other temperatures. [c] The head group volume was calculated using $v_h = v_{mol} - v_c$.

whereas the SANS curve is monotonically decreasing over the measured scattering vectors range. The IFT method gives a radius of gyration of $R_g = 21.9$ Å for the SAXS data wheras a radius of gyration of $R_g = 13.4$ Å is determined for the SANS data. Using the value $D_{max} = 52$ Å, the IFT method allows a good fit to the SAXS data with a smooth $p(r)$ function. To reach a similar result for the SANS data, the value $D_{max} = 37$ Å has to be defined. For comparison, the $p(r)$ function of the SANS data calculated with $D_{max} = 52$ Å is also shown. In the latter case, the $p(r)$ values are negative for larger values of r.

The $p(r)$ function from SANS data is symmetric and shows no tail at larger r values, which indicates a homogeneous spherical particle. In contrast, the $p(r)$ function evaluated from the SAXS data shows two peaks that are typical features for inhomogeneous particles. The difference between these results is due to the fact that the scattering-length density profile for X-rays and neutrons is significantly different. As shown in Figure 4a, in neutron scattering experiments, the solvent D_2O has a higher scattering-length density (6.38×10^{10} cm^{-2}) than the head and tail groups of the OM molecule. Hence, both head (4.0×10^{10} cm^{-2}) and tail (0.42×10^{10} cm^{-2}) groups have a negative density contrast compared with that of the solvent (6.38×10^{10} cm^{-2}). In X-ray scattering, the scattering-length density of the head group (14.8×10^{10} cm^{-2}) is higher than that of the solvent (9.41×10^{10} cm^{-2}) whereas the scattering-length density of the tail group (7.55×10^{10} cm^{-2}) is lower. Thus, in X-ray scattering, the hydrophobic core has a negative contrast relative to that of the solvent whereas the hydrophilic shell has a positive contrast, which means that these two parts have opposite signs. For this reason, oscillations of the $p(r)$ function can be seen in SAXS data at small r values.

It should be noted that Figure 4a is only a schematic description of the scattering-length density profile where the hydration water in the hydrophilic shell has not been taken into account. In reality, there is always water in the hydrophilic shell, so the average scattering-length density of the shell, ρ_s, is closer to that of the solvent, ρ_0. In contrast, the scattering-length density of the micelle core, ρ_c, is constant. Figure 4b shows how the contrast ratio of the shell and the core, $(\rho_s - \rho_0)/(\rho_c - \rho_0)$, changes with hydration number. With a hydration number of 40, the contrast ratio for neutron scattering is about 0.078, which means that the hydrophobic core has a much higher contrast than does the hydrophilic shell in neutron scattering. Consequently, in SANS, the contribution of the shell to the radius of gyration is lower than that of the micelle core. In contrast, for X-ray scattering, using the same hydration number of 40, the contrast ratio $(\rho_s - \rho_0)/(\rho_c - \rho_0)$ is -0.58, and both the shell and the core have significant contrast. In other words, the hydrophilic shell has a larger contribution in SAXS data than in SANS data. This explains why we find a larger R_g from the SAXS datathan from the SANS data.

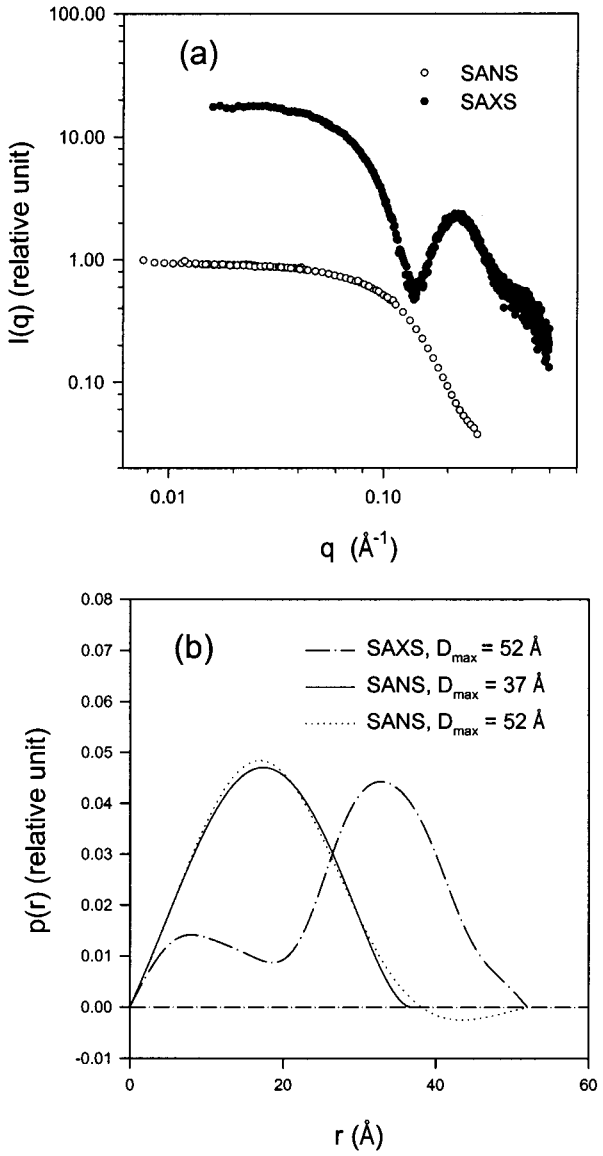

Figure 3. (a) Typical patterns of OM micelles in SANS and SAXS. Both measurements were performed in D_2O. For SANS data, $c = 92.2$ mM and $T = 25$ °C. For SAXS data, $c = 97.4$ mM and $T = 25$ °C. (b) $p(r)$ function of the scattering data shown in Figure 3a in relative units.

Structure Analysis. When evaluated from the SANS data, the $p(r)$ function, which gives an indication about the shape and size of the molecule, shows that a spherical shape is possible. Furthermore, the $p(r)$ function that is based on the SAXS data shows that a shell model could be used to describe the micelle structure. Therefore, we decided to use the monodisperse spherical shell model to fit the data to obtain more detailed structural information. In the fitting procedure, the micelle core radius R_c, the total micelle radius R_t, and the contrast ratio of the micelle core with the hydrophilic shell $(\rho_s - \rho_0)/(\rho_c - \rho_0)$ were optimized using a least-squares method. Because the solutions for SANS and SAXS experiments were not identical, the SANS and SAXS data were fitted separately.[36] Figure 5 shows an example of the fitting results we obtained using the spherical shell model. It can be seen that the fitted curves are close to the experimental data. Only at low q values are there small differences between the calculated value and the experimental SANS data, whereas for the SAXS data, a discrepancy between the experimental points and the fitted curve

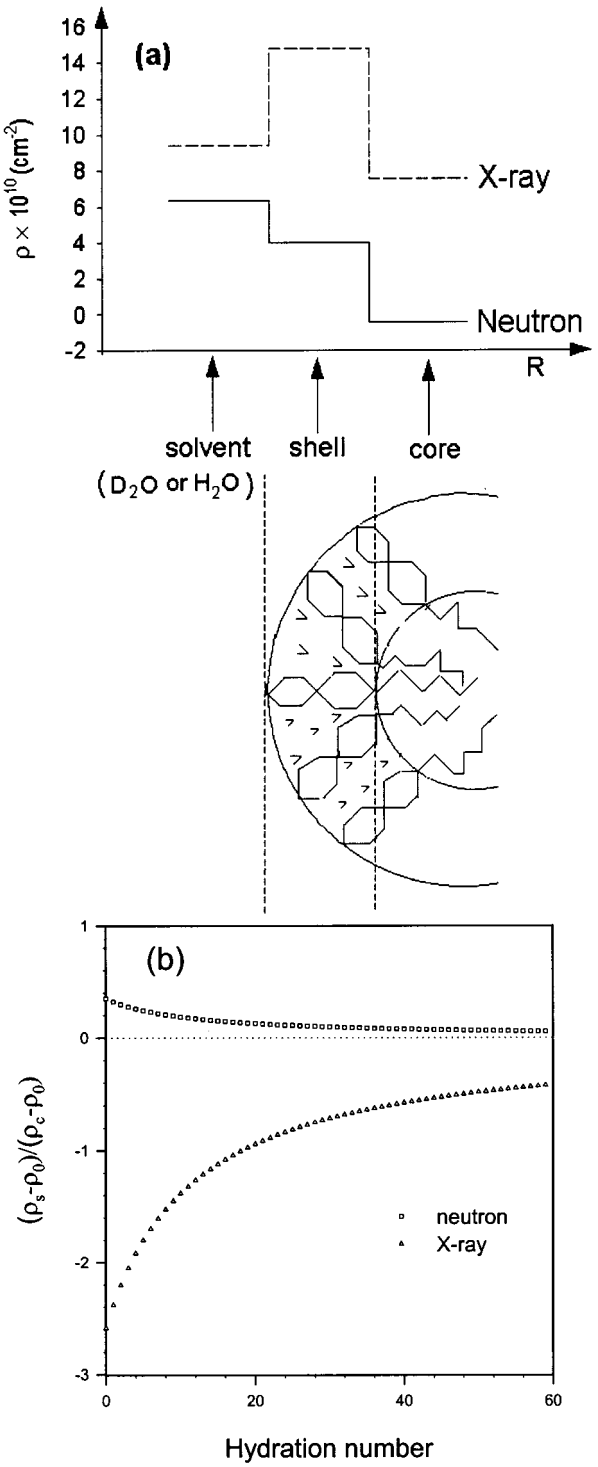

Figure 4. (a) Scattering-length density of the bulk solvent, hydrophilic shell, and micelle core. The scattering-length density is calculated by $\rho = \sum_i^n b_i/v$, where v is the volume of the head group or tail group and b_i is the scattering length of the atoms obtained from ref 41. For neutron scattering using D_2O as the solvent, seven H atoms of the OH groups in the head group were assumed to exchange with D atoms in the solvent, and this gave a value of 4.0 for the micelle shell. (The value would be 1.89 without the consideration of H−D exchange.) For simplicity, hydration water in the micelle shell was not considered in this Figure. (b) Contrast ratio of the micelle core and the hydrophilic shell considering the hydration water. The scattering-length density in the hydrophilic shell, ρ_s, was calculated by averaging the scattering-length densities of the head group and the solvent: $\rho_s = \sum_i^n b_i/(v_h + hv_{H_2O})$, where $\sum_i^n b_i$ is the summary of the scattering lengths of all atoms in the hydrophilic shell, v_h is the volume of the head group, v_{H_2O} is the volume of a water molecule, and h is the hydration number.

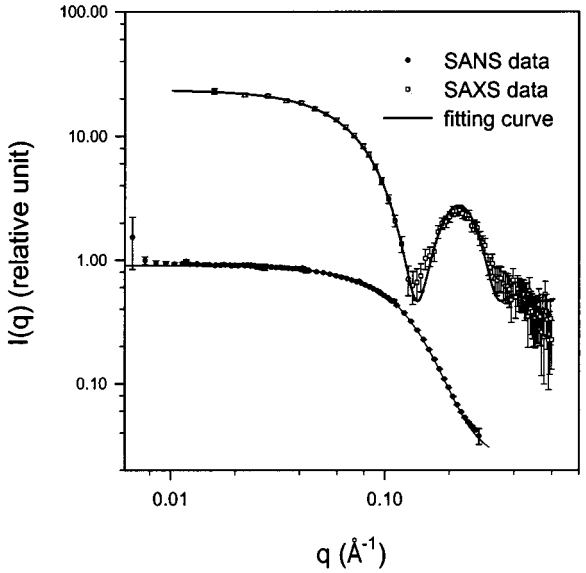

Figure 5. Fitted curves of experimental SANS and SAXS data using the spherical shell model. SANS experimental conditions: $c = 92.2$ mM; $T = 40$ °C; solvent, D_2O; SAXS experimental conditions: $c = 96.5$ mM; $T = 35$ °C; solvent, H_2O. The fitting parameters are listed in Table 2. For better visualization of the error bars and the fitting curve, only 20% of the experimental SAXS data that were used in the calculation are shown in this Figure.

in the high q region can be observed. However, this discrepancy is within the experimental error.

As a comparison, two other micelle geometries—the ellipsoidal shell model and the cylindrical shell model—were used to fit the scattering data. The results using the cylindrical shell model were poor (data not shown) and were rejected for further analysis. The ellipsoidal shell model and the spherical model gave equally good fitting results. The obtained ellipticity ϵ is approximately 1.05, indicating a nearly spherical shape. Also, the major radius of the ellipsoid is close to the sphere radius, which suggests that a spherical shell model is appropriate to use in describing the micelle shape. Thus, further structure analysis of the micelle was carried out using the spherical shell model.

The radius of micelle core R_c and the radius of the entire micelle R_t can be derived from the data. Because there is no water in the hydrocarbon core and the hydrocarbon chain volume v_c is known, one can obtain the aggregation number N_{agg} using

$$V_{core} = \frac{4}{3}\pi R_c^3 \tag{15a}$$

$$= N_{agg} v_c \tag{15b}$$

where V_{core} is the volume of hydrocarbon core of the micelle. The entire micelle consists of monomers and hydration water. Therefore, we can calculate the hydration number h by using

$$V_{mic} = \frac{4}{3}\pi R_t^3 \tag{16a}$$

$$= N_{agg}(v_{mol} + v_w h) \tag{16b}$$

where V_{mic} is the micelle volume, v_{mol} is the monomer volume, and v_w is the water molecule volume. Note that here the hydration water includes not only water molecules bound to the head groups but also free water in the hydrophilic shell.

The results of the SANS and SAXS data analyses are summarized in Table 2. Although the radii of gyration from

TABLE 2: IFT Analysis and the Spherical Shell Model Fitting Results of SANS and SAXS Data

	experimental conditions			IFT results		modeling fitting parameters				
	c (mM)	solvent	T (°C)	R_g (Å)	D_{max} (Å)	R_c (Å)	R_t (Å)	$\Delta\rho_s/\Delta\rho_c$	N_{agg}	h
SAXS	96.5	H_2O	10	20.5 ± 0.05	52	11.4 ± 0.2	23.2 ± 0.3	−0.76 ± 0.08	26	48
SAXS	96.5	H_2O	25	21.7 ± 0.07	52	11.4 ± 0.1	24.1 ± 0.1	−0.57 ± 0.01	26	58
SAXS	96.5	H_2O	35	21.7 ± 0.08	52	11.5 ± 0.1	24.0 ± 0.1	−0.58 ± 0.01	26	56
SAXS	96.5	H_2O	50	21.5 ± 0.08	52	11.4 ± 0.1	23.8 ± 0.1	−0.56 ± 0.01	25	55
SAXS	97.4	D_2O	10	21.8 ± 0.07	52	11.4 ± 0.1	24.4 ± 0.1	−0.59 ± 0.02	26	59
SAXS	97.4	D_2O	25	21.9 ± 0.06	52	11.4 ± 0.1	24.3 ± 0.1	−0.57 ± 0.01	26	58
SAXS	97.4	D_2O	35	21.6 ± 0.06	52	11.5 ± 0.1	24.2 ± 0.1	−0.57 ± 0.01	26	57
SAXS	97.4	D_2O	50	21.7 ± 0.06	52	11.5 ± 0.1	24.0 ± 0.1	−0.58 ± 0.01	26	55
SANS	51.4	D_2O	15	14.2 ± 0.03	42	11.8 ± 0.1	25.8 ± 0.2	0.073 ± 0.003	29	66
SANS	51.4	D_2O	25	14.1 ± 0.03	42	11.6 ± 0.1	25.4 ± 0.2	0.078 ± 0.003	27	64
SANS	51.4	D_2O	40	14.1 ± 0.03	42	11.7 ± 0.1	25.6 ± 0.2	0.074 ± 0.003	27	67
SANS	67.8	D_2O	25	14.0 ± 0.02	42	11.6 ± 0.1	25.3 ± 0.2	0.077 ± 0.003	27	64
SANS	92.2	D_2O	25	13.4 ± 0.02	37	11.4 ± 0.1	24.2 ±0.2	0.093 ± 0.004	25	59
SANS	92.2	D_2O	40	13.4 ± 0.02	37	11.5 ± 0.1	23.7 ± 0.2	0.108 ± 0.004	26	52
SANS	140	D_2O	20	13.2 ± 0.02	37	11.0 ± 0.1	22.2 ± 0.2	0.148 ± 0.005	23	47
SANS	140	D_2O	40	13.1 ± 0.02	37	11.0 ± 0.1	22.1 ± 0.2	0.155 ± 0.005	23	46
SANS	188	D_2O	20	12.9 ± 0.02	37	10.8 ± 0.1	21.4 ± 0.2	0.185 ± 0.005	22	43
SANS	188	D_2O	30	12.9 ± 0.02	37	10.9 ± 0.1	21.4 ± 0.2	0.183 ± 0.005	22	43
SANS	188	D_2O	40	12.9 ± 0.02	37	10.8 ± 0.1	21.3 ± 0.2	0.188 ± 0.005	21	44
SANS	188	D_2O	50	12.8 ± 0.02	37	10.8 ± 0.1	21.3 ± 0.2	0.185 ± 0.005	21	43

SANS and SAXS data by IFT are very different, the model fitting taking into account the difference in the scattering density between SANS and SAXS rendered similar results for the structural parameters.

Isotopic Solvent Effects. In the SANS experiments, D_2O was employed as the solvent to enhance the scattering contrast and reduce the incoherent background. Because D_2O has a higher density and viscosity than H_2O, the micelle structure measured in D_2O might be somehow different than the structure measured in H_2O. Because the scattering-length density of H_2O and D_2O are the same in X-ray scattering, SAXS provides the opportunity to compare the micelle structure in the two isotopic solvents. The SAXS patterns of OM in D_2O and H_2O at 35 °C are shown in Figure 6a. The differences in the $p(r)$ functions of the two systems are negligible. The radii of gyration determined by the IFT method are 21.7 and 21.6 Å for H_2O and D_2O, respectively, and the derived structural parameters are very similar (Table 2). The comparison of the $p(r)$ function in H_2O and D_2O at 25 and 50 °C gave similar results (see Figures in Supporting Information for details), which indicates that OM micelles have a similar structure in the two solvents.

Concentration Effects. It is well-known that micelle type, shape, and size can vary as functions of concentration.[29,45,46] We have studied the effect of concentration on micelle structure by SANS. The scattering patterns of OM with different concentrations at 25 °C are shown in Figure 7. As shown in Figure 7a, the absolute scattering intensity increases with the concentration, although the curves have similar patterns. For a better comparison, the data normalization was performed by dividing the scattering intensity by the micelle concentration (c − CMC). Figure 7b shows that the normalized curves at 51.4 and 67.8 mM have nearly identical scattering intensities. Also, their $p(r)$ functions are similar (see Figure 7c). In contrast, the normalized curve for 92.2 mM lies significantly below those for 51.4 and 67.8 mM. SANS curves as a function of concentration at 40 °C are shown in Figure 8. The data shown in Figures 7 and 8 follow similar trends, which suggests that micelle interactions exist at high concentration. In the modeling work, the effect of micelle interactions has been included in the calculation of the structure factor $S(q)$ (see eq 14). $S(q)$ is shown at two different concentrations in Figure 8c. At low q values, it can be seen that $S(q)$ at 188 mM is significantly lower than 1. This results in a decrease of the total scattering intensity

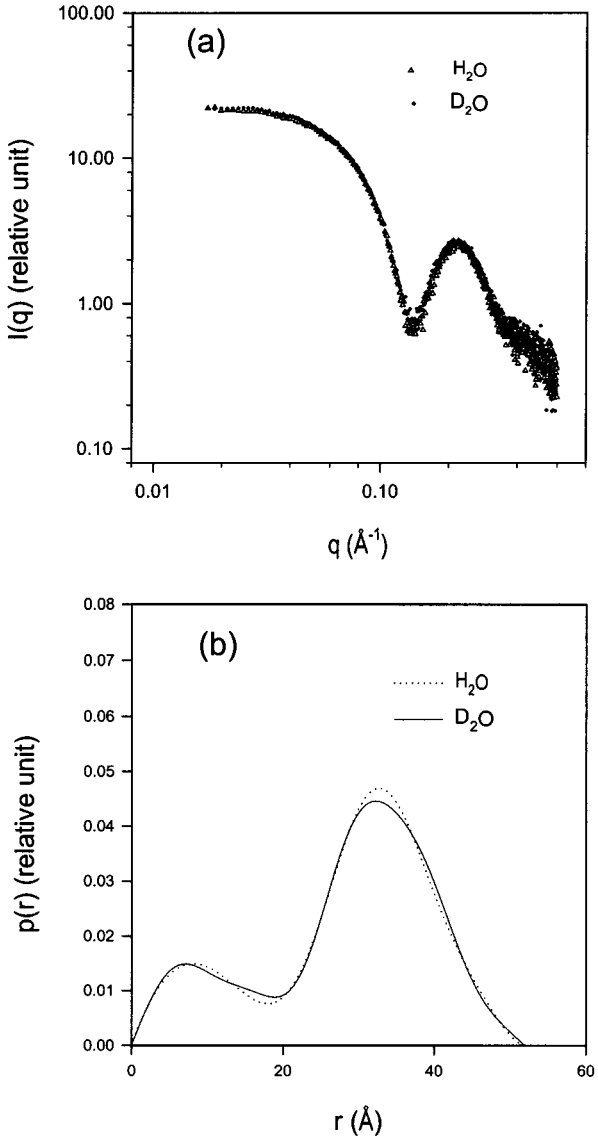

Figure 6. (a) Comparison of SAXS patterns in H_2O and D_2O. c = 96.5 mM in H_2O and 97.4 mM in D_2O. SAXS data for both samples were obtained at 35 °C. (b) $p(r)$ function of the corresponding SAXS data.

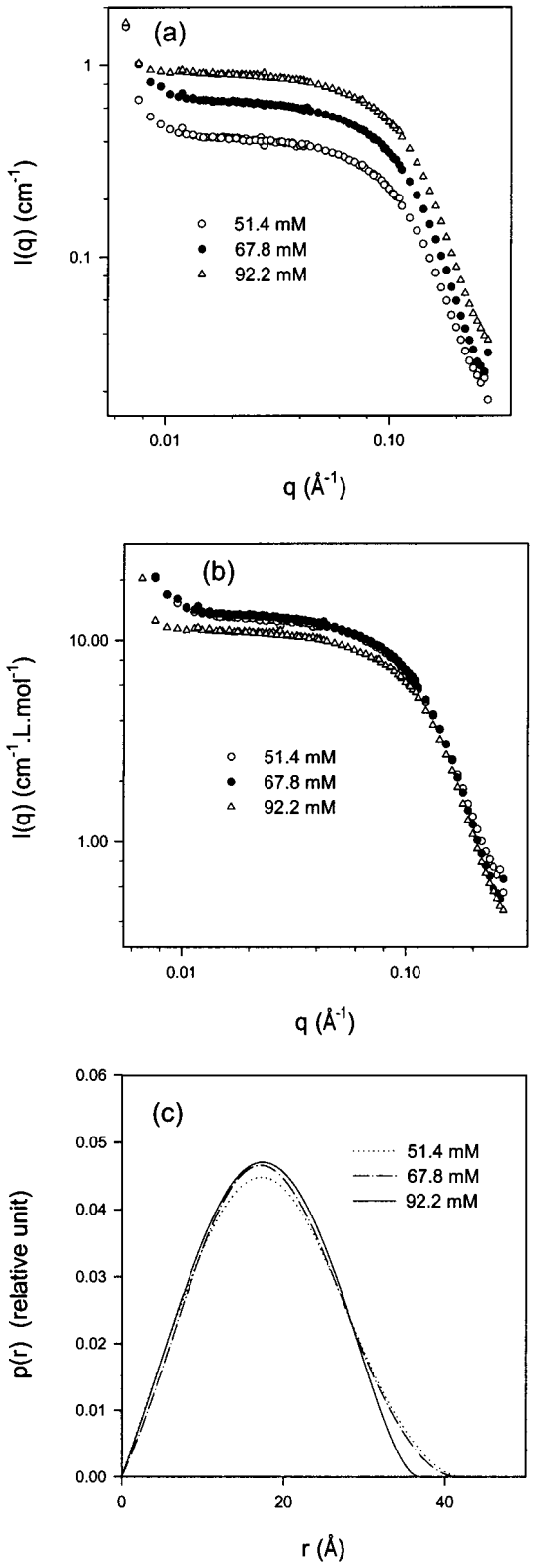

Figure 7. SANS data as a function of concentration at 25 °C. (a) Scattering data are shown on an absolute scale. (b) Scattering data were concentration normalized by dividing the intensity by (c − CMC). (c) $p(r)$ function of the corresponding data.

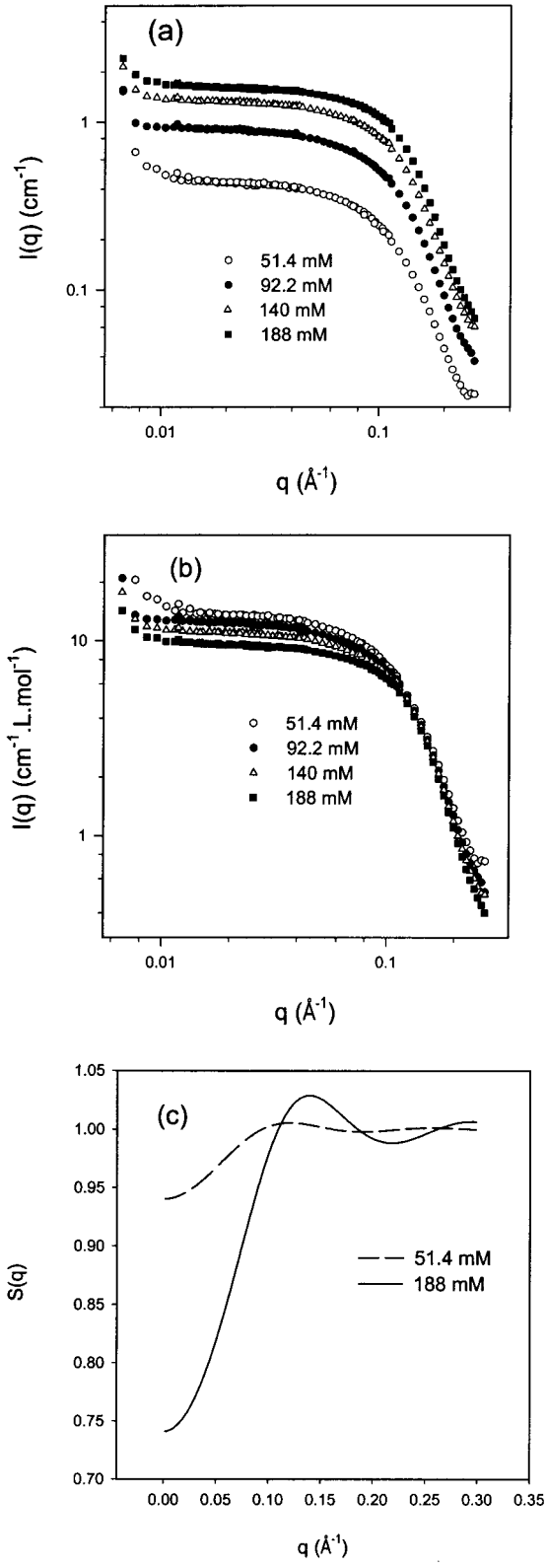

Figure 8. Effect of concentration on SANS behavior at 40 °C. (a) Scattering data are shown on an absolute scale. (b) Scattering data were concentration normalized by dividing the intensity by (c − CMC). (c) Structure factor $S(q)$ at c = 51.4 and 188 mM.

in the normalized curves (see Figure 8b). From Table 2, it can be seen that the size of the OM micelles is not sensitive to concentration and that there is no increase of the aggregation number with increasing concentration. Because of the critical packing parameter of OM, the formation of spherical micelles is more favorable than that of rod or lamellae-like micelles.[46] Also, the growth of spherical micelles is limited by the length of the alkyl chain.[29]

Temperature Effects. The behavior of some nonionic surfactants such as polyoxyethylene-based surfactants is strongly temperature dependent.[45] For example, the size of the micelles formed by a polyoxyethylene surfactant, $C_{12}E_5$, dramatically

TABLE 3: Geometric Properties and CMC of OM, DM, and OG at 25 °C[a]

	molecular volume[a] v_{mol} (Å^3)	carbon chain volume[b] v_c (Å^3)	head group volume[b] v_h (Å^3)	extended chain length[c] l_c (Å)	head group area[d] σ (Å^2)	packing parameter $v_c/(l_c\sigma)$	CMC[e] (mM)
OM	587.3	242.6	344.7	11.6	40	0.52	19.1
DM	691	350.2	340.8	18.2	44	0.43	0.13 (0.2)
OG	422.0	242.6	179.4	11.6	40	0.52	18.2 (25.1)

[a] Calculated from the partial molar volume. The value of OM was measured in the present study, the value of DM is from ref 19, and the value of OG is from ref 47. [b] See Table 1 for the calculation methods. [c] Calculated with $l_c = 1.5 + 1.265n_c$; see ref 29. [d] Head group area per molecule at the air−aqueous solution interface. These values are from ref 23. [e] Surface tension data from ref 23. The values in parentheses are from other publications. For DM, ref 19 gave a value of 0.2 mM. For OG, ref 48 gave a value of 25.1 mM.

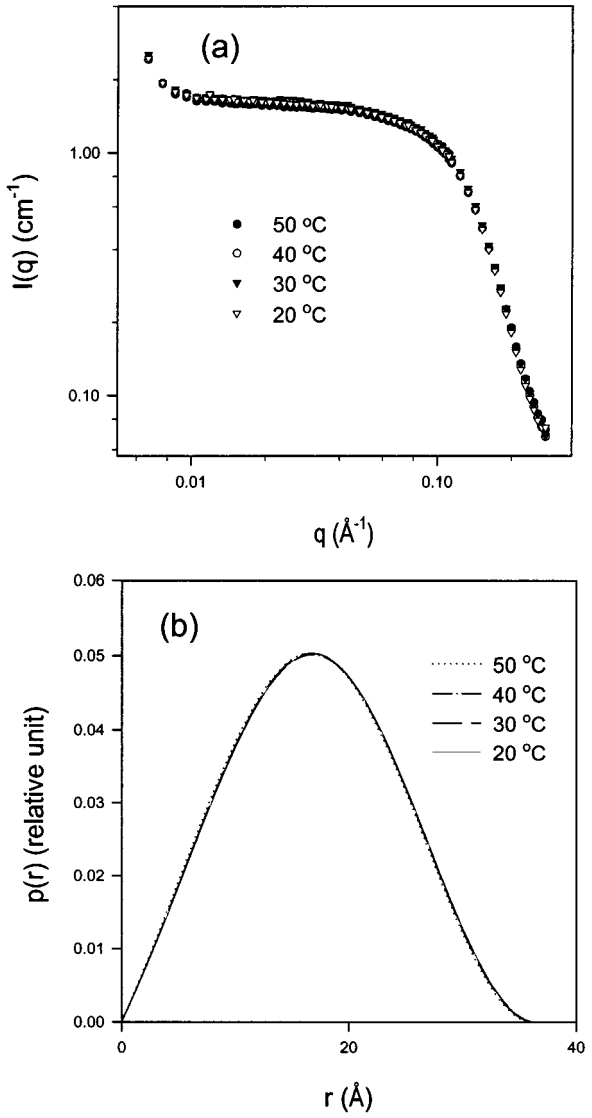

Figure 9. SANS data as a function of temperature. (a) SANS data of 188 mM OM in D_2O at different temperatures. (b) $p(r)$ function of the SANS data shown in Figure 9a.

increases as a function of temperature.[45] However, in the temperature range studied here, the effect of temperature on the OM micelle size is not obvious. As shown in Figure 9a, there are small differences in the SANS patterns for 188 mM OM from 20 to 50 °C. Also, their respective $p(r)$ functions are nearly overlapping (Figure 9b); consequently, the micelle radii are very similar. The SAXS data for 97 mM OM from 10 to 50 °C and the SANS data show similar behavior (see Supporting Information), which indicates that the size of the OM micelles is temperature-insensitive within the studied concentration and temperature regions.

TABLE 4: Comparison of the Micelle Structures of OM, DM, and OG

	aggregation number	shape	micelle size[d] whole micelle	micelle size[d] hydrocarbon core
OM[a]	26	sphere	$R = 23.7$ Å	$R_c = 11.5$ Å
DM[b]	132	oblate ellipsoid	$R = 34.4$ Å, $\epsilon = 0.59$	$R_c = 28.2$ Å, $\epsilon_c = 0.5$
OG[c]	90	cylinder	$R = 12.7$ Å, $L = 96$ Å	$R_c = 8.5$ Å, $L_c = 88$ Å

[a] Determined in the present study; $c = 92$ mM, and $T = 25$ °C. [b] Obtained from ref 19; $c = 100$ mM, and $T = 24$ °C. [c] Determined in ref 17; $c = 98$ mM, and $T = 25$ °C. [d] For OM, R is the sphere radius. For DM, R is the major radius of the ellipsoid, and ϵ is its ellipticity. For OG, R is the radius of the cylinder, and L is its length. The subscript c stands for micelle core.

Discussion

For a comparison of the structures of OM, DM, and OG, the geometric properties of these molecules are listed in Table 3. Geometric packing considerations usually give a good estimate of the micelle structure.[45,46] Because the packing parameter $v_c/(l_c\sigma)$ of OM in Table 3 is larger than 0.33, it seems that OM forms a nonspherical micelle.[44] However, analysis of the SANS and SAXS data has shown that OM micelles have a spherical shape (see Table 4 for the micelle structures of OG and DM). The packing parameters in Table 3 were calculated using the head group area σ at the air−aqueous solution interface. However, the optimal head group area σ_0 in micelles differs from this value. Using the micelle structure parameters in Table 4, the σ_0 of OM was calculated to be 65 Å^2, which is 60% higher than the value at the air−aqueous solution interface (40 Å^2).

Because OM and OG have the same hydrocarbon chain, their micelle structure difference must be due to their different head groups. It is known that there are strong short-range repulsive "hydration" forces between sugar head groups[46] that can prevent the formation of large micelles.[29] In light of their differential scanning calorimetry (DSC) results, Boyd et al. suggested that alkyl β-maltopyranoside has hygroscopic properties.[23] This indicates that there is strong binding of the two-sugar head group with water. To decrease the repulsive energy, a large optimal head group area σ_0 is required for OM. However, the attractive hydrophobic force between hydrocarbon chains requires a small head group area to decrease the attractive energy. Together, these two forces determine the optimal head group area σ_0, which gives a minimum value of the total interaction energy per glycolipid molecule.[46] Although OM and OG have the same head group area σ at the air−aqueous solution interface,[23] OM has a larger optimal head group area σ_0 than does OG because the repulsive hydration force of the two-sugar head group is higher than that of the one-sugar head group. Thus, OM forms

a spherical micelle as a result of the high hydrophilic force of its head group whereas OG forms a cylindrical micelle.

The micelle structure difference between OM and DM originates from the hydrocarbon chain difference. The 12-carbon chain of DM exerts a higher hydrophobic force than does the 8-carbon chain of OM, although they have the same head group; hence, DM forms a relative large micelle (compared to that of OM) and has an ellipsoid shape.

The hydrophobic force is known to increase with temperature. Consequently, some nonionic micelles grow with increasing temperature. For OM, there is little effect of temperature on the micelle structure in the studied temperature region. The reason may be that the opposite force, the hydrophilic force between the two-sugar head groups, also increases with temperature, which offsets the increase of the hydrophobic force.

Conclusions

The combination of SANS and SAXS investigations allows a detailed understanding of the structure of colloid particles. The IFT method of analysis and the model fitting of the scattering data show that OM micelles have a spherical shape. The micelle size does not increase with increasing concentration up to 188 mM, and the structure of the micelle is not sensitive to temperature from 10 to 50 °C. In H_2O and D_2O, OM micelles have similar structures. Comparison of the micelle structure between OM, OG, and DM shows that the hydrophilic force plays an important role in the determination of micelle structure.

Supporting Information Available: Detailed volumetric properties and additional scattering data. This material is available free of charge via the Internet at http://pubs.acs.org.

Acknowledgment. L.-Z.H. thanks Dr. P. K. Pranzas for the discussion on SAXS data treatment.

References and Notes

(1) Boullanger, P. *Top. Curr. Chem.* **1997**, *187*, 275.
(2) Lin, S.-C. *J. Chem. Technol. Biotechnol.* **1996**, *66*, 109.
(3) Von Rybinski, W.; Hill, K. *Angew. Chem., Int. Ed.* **1998**, *37*, 1328.
(4) Le Maire, M.; Champeil, P.; Moller, J. V. *Biochim. Biophys. Acta* **2000**, *1508*, 86.
(5) Aveldano, I. *Arch. Biochem. Biophys*. **1995**, *324*, 331.
(6) Baron, C.; Thompson, T. E. *Biochim. Biophys. Acta* **1975**, *382*, 276.
(7) Rosevear, P.; Van Aken, T.; Baxter, J.; Ferguson-Miller, S. *Biochemistry* **1980**, *19*, 4108.
(8) Gould, R. J.; Ginsberg, B. H.; Spector, A. A. *Biochemistry* **1981**, *20*, 6776.
(9) Almegren, M. *Biochim. Biophys. Acta* **2000**, *1508*, 146.
(10) Herman, D. C.; Lenhard, R. J.; Miller, R. M. *Environ. Sci. Technol.* **1997**, *31*, 1290.
(11) Zhang, J.-W.; Lee, S.-H.; Gross, R. A.; Kaplan, D. *J. Chem. Technol. Biotechnol.* **1999**, *74*, 759.
(12) Von Rybinski, W. *Curr. Opin. Colloid Interface Sci.* **2001**, *6*, 146.
(13) Hoffmann, B.; Platz, G. *Curr. Opin. Colloid Interface Sci.* **2001**, *6*, 171.
(14) Stubenrauch, C. *Curr. Opin. Colloid Interface Sci.* **2001**, *6*, 160.
(15) Soderman, O.; Johansson, I. *Curr. Opin. Colloid Interface Sci.* **2000**, *4*, 391.
(16) Aoudia, M.; Zana, R. *J. Colloid Interface Sci.* **1998**, *206*, 158.
(17) He, L.-Z.; Garamus, V.; Niemeyer, B.; Helmholz, H.; Wilumeit, R. *J. Mol. Liq.* **2000**, *89*, 239.
(18) Sakya, P.; Seddon, J. M.; Vill, V. *Liq. Cryst.* **1997**, *23*, 409.
(19) Dupuy, C.; Auvray, X.; Petipas, C. *Langmuir* **1997**, *13*, 3965.
(20) Zhang, L.; Somasundaran, P.; Maltesh, C. *Langmuir* **1996**, *12*, 2371.
(21) Lijeqvist, P.; Kronberg, B. *J. Colloid Interface Sci*. **2000**, *222*, 159.
(22) Lijeqvist, P.; Kronberg, B. *J. Colloid Interface Sci.* **2000**, *222*, 165.
(23) Boyd, B. J.; Drummond, C. J.; Kfodkiewska, I.; Grieser, F. *Langmuir* **2000**, *16*, 7359.
(24) Weerawardena, A.; Boyd, B. J.; Drummnond, C. J.; Furlong, D. N. *Colloids Surf., A* **2000**, *169*, 317.
(25) Mechref, Y.; El Rassi, Z. *Electrophoresis* **1997**, *18*, 912.
(26) Mechref, Y.; El Rassi, Z. *Electrophoresis* **1997**, *18*, 220.
(27) Zhang, R.-T.; Marone, P. A.; Thiyagarajan, P.; Tiede, D. M. *Langmuir* **1999**, *15*, 7510.
(28) Pastor, O.; Junquera, E.; Aicart, E. *Langmuir* **1998**, *14*, 2905.
(29) Tanford, C. *The Hydrophobic Effect: Formation of Micelle and Biological Membranes*; Wiley & Sons: New York, 1980.
(30) Cotton J. P. In *Neutron, X-ray and Light Scattering: Introduction to an Investigative Tool for Colloidal and Polymeric Systems*; Lindner P., Zemb T., Eds.; North-Holland: Amsterdam, 1991.
(31) Wignall, G. D.; Bates, F. S. *J. Appl. Crystallogr.* **1986**, *20*, 28.
(32) Pedersen, J. S.; Posselt, D.; Mortensen, K. *J. Appl. Crystallogr*. **1990**, *23*, 321.
(33) Koch, M. H. J.; Bordas, J. *Nucl. Instrum. Methods* **1983**, *208*, 461.
(34) Boulin, C. J.; Kempf, R.; Gabriel, A.; Koch, M. H. J. *Nucl. Instrum. Methods Phys. Res., Sect. A* **1988**, *269*, 312.
(35) The programs for raw SAXS data treatment can be found via the Internet at http://www.embl-hamburg.de/ExternalInfo/Research/Sax/program.html.
(36) Pedersen, J. S. *Adv. Colloid Interface Sci*. **1997**, *70*, 171.
(37) Pedersen, J. S. *Curr. Opin. Colloid Interface Sci.* **1999**, *4*, 190.
(38) Glatter, O. *J. Appl. Crystallogr.* **1977**, *10*, 415.
(39) Glatter, O.; Kratky, O. *Small-Angle X-ray Scattering;* Academic Press: London, 1982.
(40) Kotlarchyk, M.; Chen, S. H. *J. Chem. Phys.* **1983**, *79*, 2461.
(41) Feigin, L. A.; Svergun, D. I. *Structure Analysis by Small-Angle X-ray and Neutron Scattering;* Plenum Press: New York, 1987.
(42) Percus, J. K.; Yevick, G. *Phys. Rev.* **1958**, *110*, 1.
(43) Kinning, D. J.; Thomas, E. L. *Macromolecules* **1984**, *17*, 1712.
(44) Bevington, B. R. *Data Reduction and Error Analysis for Physical Sciences*; McGraw-Hill: New York, 1969.
(45) Jönsson, B.; Lindman, B.; Holmberg, K.; Kronberg, B. *Surfactants and Polymers in Aqueous Solution*; Wiley & Sons: New York, 1998.
(46) Israelachvili, J. N. *Intermolecular and Surface Forces*, 2nd ed.; Academic Press: London, 1992.
(47) Antoneli, M. L.; Bonicelli, M. G.; Ceccaroni, G.; Mesa, C. L.; Seta, B. *Colloid Polym. Sci.* **1994**, *272*, 704.
(48) Shinoda, K.; Yamanaka, T.; Kinoshita, K. *J. Phys. Chem.* **1959**, *63*, 648.